RSC Sustainability

ROYAL SOCIETY OF CHEMISTRY

PAPER

View Article Online
View Journal | View Issue

Cite this: *RSC Sustainability*, 2025, **3**, 3009

Modification of calcium carbonate from blue mussel shells with copper oxide nanoparticles†

Sachel Christian-Robinson,[a] Fanqi Kong,[b] E. Bradley Easton [b] and Francesca M. Kerton [*a]

Received 14th March 2025
Accepted 12th May 2025

DOI: 10.1039/d5su00188a

rsc.li/rscsus

Biogenic calcium carbonate byproducts can be repurposed as valuable materials. In this study, we prepared copper oxide nanocomposites of a calcite material (soft calcite) derived from Newfoundland blue mussel (*Mytilus edulis*) shells. The nanocomposites were synthesized *via* the simultaneous reduction of copper(II) salts using a Newfoundland partridge berry (*Vaccinium vitis-idaea*) extract and the incorporation of the copper-containing nanoparticles onto the surface of the soft calcite. The syntheses were carried out under varying conditions of time, temperature and pH to optimise the incorporation of copper in the composites, with XPS studies providing insights into copper speciation. Among the different nanocomposites, the nanocomposite prepared at room temperature in the presence of NaOH for 48 h had the highest copper content. This nanocomposite was selected for further investigation of catalytic activity through the reduction of 4-nitrophenol in the presence of sodium borohydride. Appreciable reduction could be attained in 20 min.

Sustainability spotlight

The aquaculture industry plays a significant role in achieving the United Nation's Sustainable Development Goal of Zero Hunger (UN SDG 2). However, waste generated by this industry must be managed sustainably. Mussel shells, primarily composed of calcium carbonate, present a valuable opportunity for resource utilization. Effectively using this material can divert waste away from landfills and the ocean, reducing the environmental impact and addressing UN SDGs 14 (life below water) and 15 (life on land). Additionally, this approach helps in the advancement towards a more circular economy and UN SDG 12 (responsible consumption and production).

Introduction

Calcium carbonate is ubiquitous in everyday life, from construction materials including limestone and marble, to antacid medicines and treatments for acidic soils. It is the main component of eggshells and mollusk shells, including those of snails (gastropods) and mussels (bivalves). Many researchers have been investigating uses for waste shells from the food industry with the aim of achieving a circular economy and finding new uses for the by-products.[1–3] We have been studying the chemistry of calcium carbonate from blue mussel (*Mytilus edulis*) shells and discovered a distinct, unusual form of calcite, which we termed soft calcite (SC) to distinguish it from the tightly bound bundles of calcite crystals found in natural shells. This unique material consists solely of needle-like calcite (unlike the precursor shells, which consist of both aragonite and calcite polymorphs) arranged in a nest-like morphology, giving it a unique texture and properties.[4,5] Previously, we demonstrated the use of this material for dye remediation, but just like other calcium carbonate materials derived from biogenic sources, it fell short of requirements for practical 'usage' due to a lack of surface functional groups.[5–9] However, this lack of functionality on the surface of soft calcite makes it a promising candidate for various kinds of modifications.

Modifiers, including silane (–Si–OR) and titanate coupling agents, silicates, aluminates, and organic acids, have been used in modifying calcium carbonate surfaces, although most papers have focused on non-biogenic calcium carbonate sources for these types of surface functionalizations.[10–12] For bio-derived calcium carbonate, most frequently obtained from chicken eggshells, modification with metal salts and metal-based nanoparticles (MNPs) has been shown to give it valuable properties.[13–18] In some cases, plant extracts have been used as a green approach in synthesizing MNPs for the formation of bio-nanocomposites (bio-NCs) (Fig. 1).[19–23]

Inspired by this research, we undertook investigations to modify mussel shell-derived calcite with copper oxide nanoparticles using an extract from locally sourced berries, namely

[a]*Department of Chemistry, Core Science Facility, Memorial University of Newfoundland, 45 Arctic Ave, St. John's, NL, Canada, A1C 5S7*

[b]*Electrochemical Materials Lab, Faculty of Science, Ontario Tech University, 2000 Simcoe Street North, Oshawa, ON, Canada, L1G 0C5. E-mail: fkerton@mun.ca*

† Electronic supplementary information (ESI) available. See DOI: https://doi.org/10.1039/d5su00188a

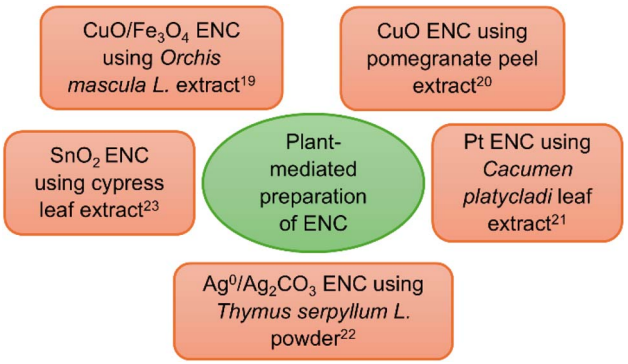

Fig. 1 Plant extract-mediated preparation of eggshell nanocomposites (ENCs).

Newfoundland partridge berries (*Vaccinium vitis-idaea*). We also screened the composite materials for their catalytic activity.

Materials and methods

Chemical and material supply

Whole blue mussels (*Mytilus edulis*) and whole partridge berries (*Vaccinium vitis-idaea*) were obtained from Sobeys Supermarket in St. John's, Newfoundland and Bidgoods Supermarket in Goulds, Newfoundland. A Bioquochem (BQC) anthocyanin test kit was obtained from Cosmo Bio (Carlsbad, CA, USA). Copper(II) chloride dihydrate ($CuCl_2 \cdot 2H_2O$) and copper(II) sulfate ($CuSO_4$) for nanocomposite synthesis were obtained from BDH Chemicals and JT Baker Chemical Co. (*via* Avantor/VWR Canada). Copper(I) oxide and copper(II) oxide were obtained from Sigma-Aldrich.

Preparation of the berry extract

Partridge berry extraction was adapted from Bhullar *et al.*[24] 20.0 g of berries were blended in 200 mL of deionized water and then sonicated for 3 × 15 min. After extraction, the partridge berry extract (PBE) was centrifuged for 30 min at 7000 rpm, followed by filtration using Whatman no. 1 filter paper. Anthocyanin contents were assessed using a Bioquochem (BQC) anthocyanin assay kit. Absorbances were determined by UV/Vis spectroscopy at 510 nm and 700 nm. The anthocyanin contents were determined as per the method outlined in the ESI.†

Synthesis of nanocomposites

For the synthesis of copper oxide nanocomposites, 1.00 g of soft calcite was mixed with 0.40 g of copper salt and 50 mL of PBE at 300 rpm on a hotplate stirrer. Syntheses were carried out under reflux at 80 °C for 3 h or 24 h, or at 25 °C for 24 h or 48 h. For the samples prepared at elevated temperatures, the reaction mixtures were allowed to cool to room temperature. All nanocomposite materials were isolated by filtration, washed with deionized water (30 mL) and ethanol (30 mL), and dried in an oven at 60 °C. The prepared soft calcite nanocomposites are identified as SCNC-*x*-*y*, where *x* represents the synthesis time in hours, and *y* is the temperature in °C.

Nanocomposite characterization

The concentrations of copper in the NCs were determined using a PerkinElmer 5300 DV inductively coupled plasma optical emission spectrometer (ICP-OES) in Memorial University's C-CART department and a Thermo Scientific iCE 3000 series Atomic Absorption Spectrometer (AAS). The samples were prepared by digesting 0.05 g of nanocomposite material in 1 mL of trace metal grade nitric acid at 90 °C for 2 h in an oven. The samples were allowed to cool to room temperature and underwent a series of dilutions with Milli-Q® ultrapure water prior to analysis.

An FEI 650 FEG scanning electron microscope (SEM) with a voltage of 15 kV and a 14.7 mm working distance was used to image the composite materials. For this analysis, a small sample amount was deposited on SEM conductive carbon tape and then gold-coated to minimize electronic interferences during imaging. Transmission electron microscopy (TEM) was performed using a Tecnai Spirit TEM equipped with a 4-megapixel AMG digital camera at 80 kV. Approximately 0.5 mg of sample was dispersed in 500 μL of absolute ethanol. The samples were sonicated for 10–30 min to disperse the calcite crystals within the ethanol. 5 μL of the dispersed sample was deposited on a 300-mesh Formvar/carbon supported copper TEM grid and allowed to dry for a few minutes before analysis. Nanoparticle sizes were determined using ImageJ software.

Copper species present in the NCs were further characterized by X-ray Photoelectron Spectroscopy (XPS) using a Thermo Scientific Nexsa instrument equipped with a monochromatic Al K_α X-ray source (1486.7 eV). The binding energies obtained were corrected with respect to the adventitious carbon peak at 284.5 eV. Peaks were identified and fitted according to the NIST database.[25]

Ultraviolet/visible (UV-Vis) spectral analyses were performed using an Agilent Technologies Cary 100 UV-Vis spectrophotometer equipped for diffuse reflectance spectroscopy (DRS). The spectra were obtained over a wavelength range of 200 to 800 nm with a spectral bandwidth (SBW) of 2 nm. Fourier transform infrared (FTIR) spectra were obtained using a Bruker Invenio-R FTIR spectrometer in attenuated total reflectance (ATR) mode. Scans were performed between 400 and 4000 cm^{-1} with 32 scans.

Powder X-ray diffraction (PXRD) was performed using a Rigaku MiniFlex 600 with Cu K_α radiation (40 kV, 15 mA). Scans were performed in continuous mode at 2° min^{-1} with a step size of 0.020° within the 2θ region of 3.000 to 90.000°.

Catalytic reduction of 4-nitrophenol in the presence of sodium borohydride ($NaBH_4$)

In a typical reaction, 500 μL of 4-nitrophenol (5.00×10^{-4} M) was mixed with 4 mL of D.I. water, followed by the addition of 500 μL of $NaBH_4$ (5.00×10^{-2} M). 3 mL of this solution was then added to 1.5 mg of catalyst (SCNC-48-25B, see Table 1 for details of the catalyst) in a cuvette of pathlength 1 cm. The reaction was monitored by UV-Vis spectroscopy using a DH-2000 Bal UV-Vis spectrophotometer (Ocean Optics) operated by Oceanview software. Experiments were carried out at room temperature

Table 1 Copper content and Cu^{+}/Cu^{2+} ratio of NCs prepared under different conditions

Nanocomposite	Time (h)	Temperature (°C)	Copper content[c] (mg g^{-1})	Cu^{+}/Cu^{2+} ratio[d]
SCNC-24-80	24	80	91.48 ± 8.13	0.81
SCNC-24-80S[a]	24	80	59.62 ± 8.87	0.74
SCNC-3-80	3	80	24.91 ± 7.35	0.68
SCNC-24-25	24	25	7.04 ± 0.29	0.71
SCNC-48-25	48	25	10.48 ± 1.45	0.81
SCNC-48-25B[b]	48	25	100.77 ± 3.44	1.31

[a] Anhydrous $CuSO_4$ used. [b] NaOH added. [c] Obtained by ICP-OES and FAAS. [d] Based on XPS data.

without stirring. The catalyst was recycled by carefully removing the spent solution, then gently rinsing the catalyst in the cuvette twice with D.I. water. Residual moisture was allowed to evaporate at room temperature before the next cycle.

Results and discussion

Factors influencing NP synthesis

The formation of NPs can be greatly influenced by temperature and time.[26] For our system, syntheses were carried out at either room temperature (RT, 25 °C) or 80 °C. These conditions were chosen based on commonly reported temperatures for synthesizing Cu NP species and bio-NCs of Cu NP species in the literature.[19,20,27] NCs synthesized at RT resulted in low incorporation of Cu NPs, with little difference in the amount of Cu between those prepared over 24 h or 48 h (Table 1). The Cu content determined in NCs prepared at RT over 24 h and 48 h was 7.04 ± 0.29 mg g^{-1}(SCNC-24-25) and 10.48 ± 1.45 mg g^{-1} (SCNC-48-25), respectively. It should be noted that the exact speciation of the copper cannot be determined *via* ICP-OES, and the Cu content detected could be from either NPs (as seen for the NCs prepared at elevated temperatures discussed below) or from adsorption of the precursor ionic copper salts. NPs in the NCs prepared at RT could not be confirmed *via* SEM and TEM imaging due to the low concentrations and the presumably sparse nature of species on the surface of the calcite crystals. However, at an elevated temperature of 80 °C, Cu concentration in the samples was significantly higher, with a Cu content of 91.48 ± 8.13 mg g^{-1} (SCNC-24-80), around 8 to 13× higher than NCs synthesized at RT (Table 1). Under SEM imaging, these NPs exhibited a somewhat angular morphology and were deposited unevenly on the calcite needles (Fig. 2). TEM imaging revealed these NP structures to be agglomerations of NPs that were individually mostly spherical in nature, with an average size of 10.7 ± 0.2 nm. The maximum attainable Cu concentration in our composite was 129.70 mg g^{-1}; however, considering the need for energy conservation, no reaction was carried out beyond 24 h at elevated temperatures. For comparison, however, we wanted to assess the Cu NP formation at 80 °C for 3 h, since Nasrollahzadeh *et al.*[19] reported Cu NC formation in as little as 3 h. After 3 h, the Cu content in our NCs was determined as 24.91 ± 7.35 mg g^{-1} (SCNC-3-80), almost 4× less than the Cu content found in samples prepared over 24 h at the same temperature (SCNC-24-80). Changing the Cu precursor from $CuCl_2 \cdot 2H_2O$ to anhydrous $CuSO_4$ (SCNC-24-80S) at 80 °C for 24 h resulted in 1.5× less formation of NPs, with much lower dispersion as seen by SEM imaging. TEM imaging showed that these NPs agglomerated (Fig. 3). The average particle size was much larger than those formed from reduction of $CuCl_2 \cdot 2H_2O$, with a mean value of 28.2 ± 1.2 nm. Others have also reported differences in MNP sizes when the precursor salt changes for the synthesis.[28] We note that agglomeration may also have been caused by sonication used to disperse the nanocomposite during TEM sample preparation.

To test whether pH had an effect on NP formation, NaOH was added to increase the pH from 2.5 to 11.8, and the reaction mixture was stirred at room temperature for 48 h. The addition of NaOH significantly increased the concentration of the Cu NP species incorporated into the composite and even surpassed the

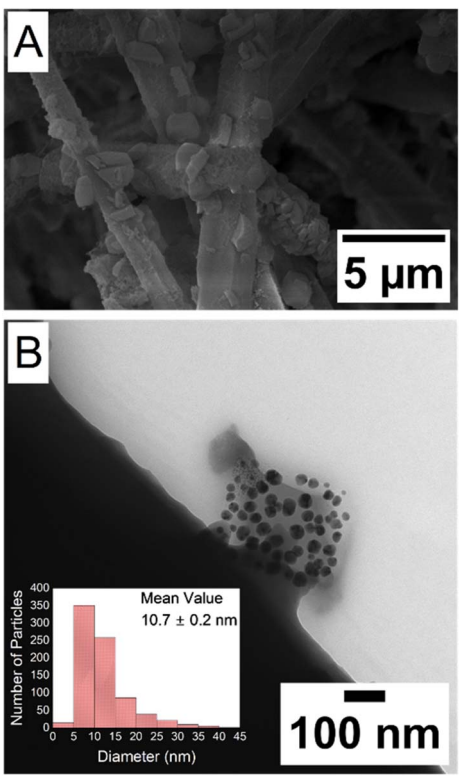

Fig. 2 (A) SEM image of SCNC-24-80 at 5 µm; (B) TEM image of SCNC-24-80 at 100 nm.

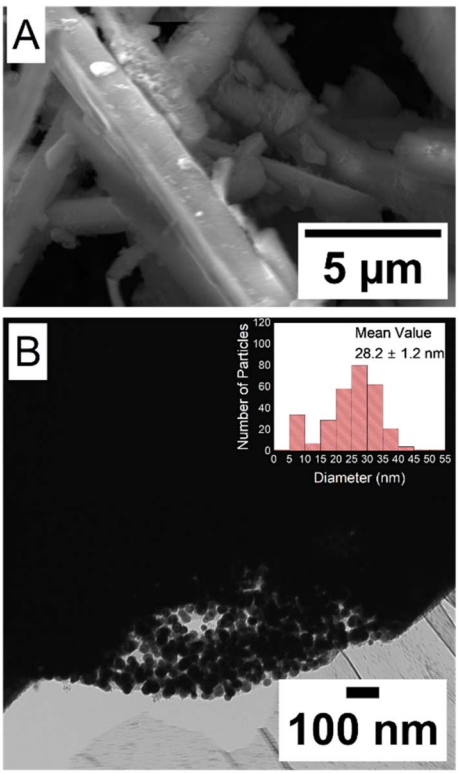

Fig. 3 (A) SEM image of SCNC-24-80S at 5 μm; (B) TEM image of SCNC-24-80S at 100 nm.

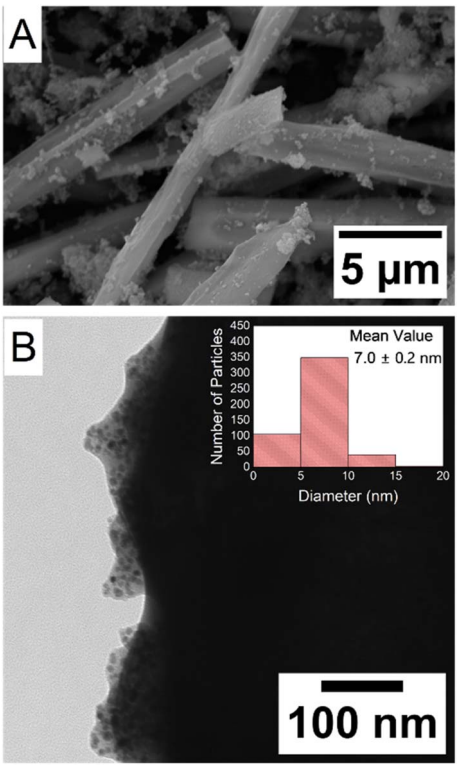

Fig. 4 (A) SEM image of SCNC-48-25B at 5 μm; (B) TEM image of SCNC-48-25B at 100 nm.

amount in the sample prepared at 80 °C over 24 h (Table 1). SEM and TEM imaging showed that the NPs formed were much smaller than SCNC-24-80 and SCNC-24-80S, with a mean value of 7.0 ± 0.2 nm (Fig. 4). Others have also reported size reductions in Cu NP species when pH was increased during their synthesis. For example, Rajesh *et al.* and Amjad *et al.* reported reductions from 23 to 12 nm and from 18 to 9 nm, respectively, when pH was increased from 6 to 10, although subsequent increases in size were observed at pH > 11.[29,30] For plant mediated reductions, the optimum pH was generally reported to be between pH 8–9, but the particular plant extract is an important factor.[28]

Spectroscopic analyses of NCs

The XRD data for NCs were similar to those for the unmodified SC material as shown in the X-ray diffractograms (Fig. 5), with no distinct evidence of any Cu species. To further investigate, XPS measurements were performed, which revealed the presence of two distinct Cu species in our samples (Fig. 6). A set of doublet peaks for $Cu2p_{3/2}$ and $Cu2p_{1/2}$ were observed at 933.15 eV and 952.71 eV, respectively, which correspond to the Cu^{+} species with a spin–orbit splitting of 19.56 eV while another set of doublet peaks were observed at 935.15 eV and 955.0 eV for the Cu^{2+} species with a splitting of 19.85 eV. Finally, shake-up satellite peaks were observed at 940.0 eV, 944.1 eV and 963.2 eV, which were characteristic of Cu oxide species such as Cu_2O and CuO.[31] We were also able to confirm the absence of Cu^{0} species due to the lack of a secondary shoulder peak in the Cu LMM Auger spectra, which would appear at a binding energy of 569.0 eV in addition to the Cu^{+} peak at 571.6 eV (Fig. S1†).[32] Additionally, the XPS data were used to determine the Cu^{+}/Cu^{2+} ratios in the samples (Table 1). The ratios ranged from 0.68 to

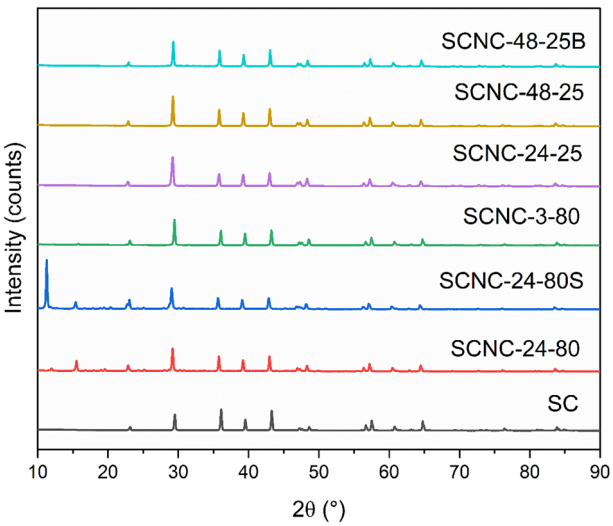

Fig. 5 X-ray diffractograms of soft calcite/copper oxide NCs and the control sample (bottom to top: black, soft calcite (SC) unmodified as the control sample; red, SCNC-24-80; blue, SCNC-24-80S; green, SCNC-3-80; purple, SCNC-24-25; yellow, SCNC-48-25; aqua, SCNC-48-25B).

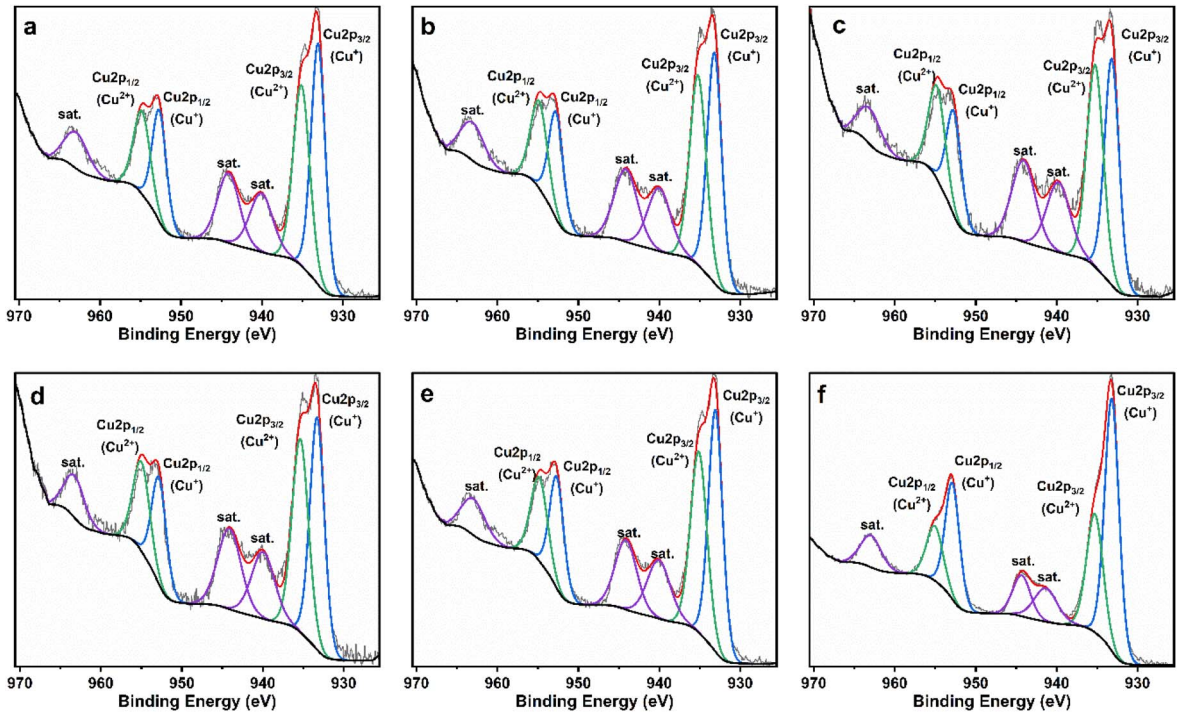

Fig. 6 XPS spectra of (a) SCNC-24-80, (b) SCNC-24-80S, (c) SCNC-3-80, (d) SCNC-24-25, (e) SCNC-48-25 and (f) SCNC-48-25B.

0.81 for NCs SCNC-24-80, SCNC-24-80S, SCNC-3-80, SCNC-24-25, and SCNC-48-25. A higher Cu^{+}/Cu^{2+} ratio of 1.31 was observed for SCNC-48-25B, where the formation of more Cu_2O relative to CuO was likely due to the synthesis being performed under basic conditions.

Following the confirmation of Cu_2O and CuO in the samples by XPS, control mixtures were prepared using commercially available bulk Cu_2O and CuO powders with SC in similar ratios to those in NCs SCNC-24-25, SCNC-24-80 and SCNC-48-25B. SCNC-24-25 was chosen for its low Cu content, SCNC-24-80 for its high Cu content, and SCNC-48-25B for its higher Cu_2O content. These control samples were labeled SC–Cu_2O–CuO(A), SC–Cu_2O–CuO(B) and SC–Cu_2O–CuO(C), respectively, and were analyzed by XRD (Fig. S2†). The XRD spectra revealed additional peaks in the control samples SC–Cu_2O–CuO(B) and SC–Cu_2O–CuO(C) between 35° and 45°, but no such peaks were observed in SC–Cu_2O–CuO(A). The strongest signal for the Cu oxide species appeared around 36.38° and 36.36° for both SC–Cu_2O–CuO(B) and SC–Cu_2O–CuO(C), respectively, corresponding to the combined effects of Cu_2O (36.38°) and CuO (36.46°), but with a stronger signal from the Cu_2O species (Fig. S2–S7†). Very weak signals were observed at 35.52° and 35.48° for SC–Cu_2O–CuO(B) and SC–Cu_2O–CuO(C), respectively, corresponding to CuO (35.58°); at 38.68° and 38.70° for SC–Cu_2O–CuO(B) and SC–Cu_2O–CuO(C), respectively, corresponding to CuO (38.78°); and at 42.26° and 42.24° for SC–Cu_2O–CuO(B) and SC–Cu_2O–CuO(C), respectively, corresponding to the combined signals of Cu_2O (42.26°) and CuO (42.34°), with a stronger contribution from Cu_2O. The presence of these peaks in the control sample but not in the NCs, particularly those with higher Cu content, suggests that the size of the particles may have significantly affected diffraction intensities. Bulk samples behave differently compared with NP species. It has been noted that as particle size decreases, XRD sensitivity decreases and results in peak broadening.[33] As a result, the strong calcite signals dominate the diffractograms of the nanocomposites reported here and lead to any weak diffraction intensities from copper oxide NPs becoming buried in the baseline.

For NCs prepared at elevated temperature, we observed additional XRD peaks between $2\theta = 11.28°$ and 15.76°. These

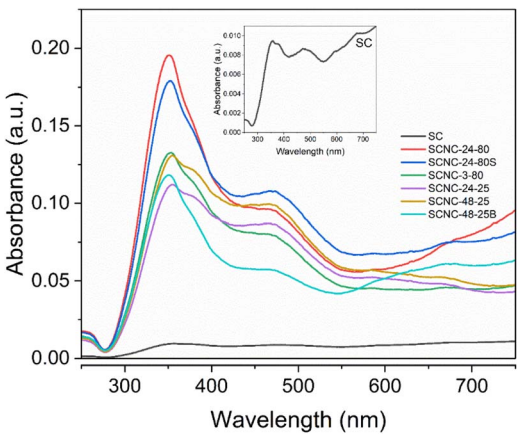

Fig. 7 Absorption spectra from diffuse reflectance spectroscopy for soft calcite/copper oxide NCs and the control sample (black, soft calcite (SC) unmodified as the control sample; red, SCNC-24-80; blue, SCNC-24-80S; green, SCNC-3-80; purple, SCNC-24-25; yellow, SCNC-48-25; aqua, SCNC-48-25B).

peaks do not match those of the Cu starting materials, which have their lowest peaks at $2\theta = 16.34°$ for $CuCl_2 \cdot 2H_2O$ and $2\theta = 17.38°$ for $CuSO_4$ (Fig. S8†), nor those of Cu_2O/CuO, which had their lowest peaks at $2\theta = 29.52°$ for Cu_2O (Fig. S6†) and $2\theta = 29.60°$ for CuO (Fig. S7†). Using MDI JADE software, we were unable to identify the origin of these peaks within the ICDD PDF-2 database. It is possible that these additional peaks indicate the formation of new crystalline species in the samples prepared at 80 °C, which may result from components in the extract and thus not appear in the ICDD PDF-2 database. The FTIR spectra for these samples also showed artifacts not present in the RT samples, which we attribute to plant-derived components (Fig. S9†). In particular, a shoulder is seen on the carbonate stretch at approximately 1556 cm^{-1}. Further research would be required to fully understand the nature and origin of these low 2θ diffraction peaks.

The NCs were all colored powders, some appearing light brown, dark brown or greenish-grey, and therefore, UV-Vis spectroscopy was performed. Analysis by DRS showed very low absorption signals for SC (Fig. 7), as expected for a colorless solid. Three absorption bands were identified, resulting in peaks at 357 nm (accompanied by a shoulder at 377 nm) and another peak at 476 nm. From 550 nm to 750 nm, there was a gradual increase in absorbance, surpassing the intensity of the previous peaks. Additionally, a shoulder appeared at 677 nm. All NCs exhibited significantly higher absorptions than SC, and those prepared at 80 °C showed higher absorption intensities overall. In the NCs, the following patterns were observed: SCNC-24-80 and SCNC-24-80S exhibited peaks in the regions of 350 and 470 nm with a gentle upward slope from 550 nm; SCNC-3-80 had peaks in the regions of 350 and 470 nm, with absorbance levelling off from 550 nm; SCNC-24-25 and SCNC-48-25 showed similar overlapping peaks to SC at around 350 and 380 nm, and a peak at 470 nm with a gentle downward slope from 550 nm; and SCNC-48-25B exhibited peaks around 350 and 470 nm and an additional peak at 670 nm (Fig. 7, S12 and Table S1†). The shoulder peaks observed in SC, SCNC-24-25 and SCNC-48-25 were absent in samples with higher Cu content. Furthermore, the ratio of the peak intensity at ~350 nm to that at ~470 nm was higher in samples with greater Cu content (Table 2). Additionally, the slope (intensity) of the absorbance from 550 nm onward appeared to correlate with the amount of Cu in the samples. NCs with the lower Cu content showed a gently downward-sloping trend, NCs with intermediate Cu levels showed a flat profile, and those with the higher Cu content displayed an upward slope. The peak in the spectrum for SCNC-48-25B ~670 nm could be due to higher [Cu^+], which was observed exclusively in this sample.

Table 2 Relative intensities of absorption peaks at ~350 nm and ~470 nm in DRS spectra

	Peak intensity		
Material	~350 nm	~470 nm	$I_{(\sim 350\ nm)}/I_{(\sim 470\ nm)}$[a]
SC	0.0095	0.0086	1.1
SCNC-24-80	0.195	0.096	2.0
SCNC-24-80S	0.179	0.108	1.7
SCNC-3-80	0.133	0.079	1.7
SCNC-24-25	0.113	0.086	1.3
SCNC-48-25	0.131	0.099	1.3
SCNC-48-35B	0.118	0.057	2.1

[a] I represents peak intensity.

Comparison of bio-NCs containing Cu species

We compared our prepared NCs, SCNC-24-80 (entry 1) and SCNC-48-25B (entry 2), to other similar plant-mediated bio-NCs of calcium carbonate (Table 3). For these NCs, $CuCl_2 \cdot 2H_2O$ was the copper precursor, and plant components were extracted using D.I. water. Both our synthesis and that of Nasrollahzadeh *et al.*[19] (entry 3) involved one-pot syntheses. In contrast, Sajadi *et al.*[20] (entry 4), prepared their bio-NCs in a three-step process: $CuCl_2 \cdot 2H_2O$ was first reduced to Cu NPs, then heated to form CuO, which was subsequently incorporated into the eggshell using water as the solvent.

Our NCs exhibited distinct morphologies compared to those reported in previous studies. Nasrollahzadeh *et al.*[19] presented SEM data, which showed Cu NPs deposited onto a porous eggshell structure. TEM imaging revealed that these NPs were spherical in nature, with smaller particle sizes than those of our NCs (entry 3). Sajadi *et al.*[20] reported the formation of spherical CuO NPs, which were approximately 3–6× larger than both the NPs reported by Nasrollahzadeh *et al.*[19] and those in the current

Table 3 Comparison of bio-NCs containing Cu species from literature sources

Nature of nanocomposite	Reductant	Time (h)	Temp. (°C)	Cu concentration (mg g^{-1})	NP particle size (nm)	Ref.
Soft calcite/Cu_2O/CuO	Partridge berry extract	24	80	91.48 ± 8.13	10.7 ± 0.2	Current work
Soft calcite/Cu_2O/CuO	Partridge berry extract, NaOH	48	25	100.77 ± 3.44	7.0 ± 0.2	Current work
Eggshell/Cu	*Orchis mascula* L. extract	3	70	110.5	5	19
Eggshell/CuO[a]	Pomegranate peel extract, NaOH	24	80	ND[b]	30	20

[a] CuO NPs were first prepared, then incorporated into the eggshell structure in the presence of water. [b] Not disclosed.

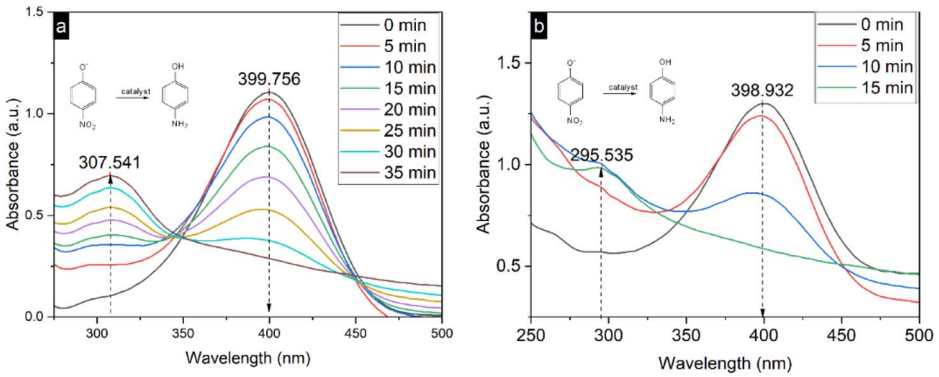

Fig. 8 Reduction of 4-nitrophenol (a) in the presence of $NaBH_4$ stabilized by NaOH and (b) $NaBH_4$ without stabilization.

study. Their SEM images displayed deposits of NPs on a rugged calcium carbonate surface containing very small pores.

Catalytic reduction of 4-nitrophenol in the presence of sodium borohydride ($NaBH_4$)

The catalytic activity of MNPs and MNCs in aqueous systems is often evaluated through the reduction of 4-nitrophenol.[34] 4-Nitrophenol reduction is important both environmentally and industrially because it is more toxic in environmental settings compared to its reduced form, 4-aminophenol. Additionally, 4-aminophenol is an important intermediate in the pharmaceutical industry.[35] To assess 4-nitrophenol reduction, we chose our SCNC-48-35B catalyst because it had the largest amount of Cu(I) within it. The progress of the reduction of 4-nitrophenol could be assessed directly by UV-Vis spectroscopy. 4-Nitrophenol exhibits a peak at 321 nm, but in the presence of $NaBH_4$, a 4-nitrophenolate ion is formed, which has a peak around 400 nm remains stable in the absence of a catalyst (Fig. S13†). In the presence of the catalyst, the progress of the reduction could be characterized by the disappearance of the peak around 400 nm

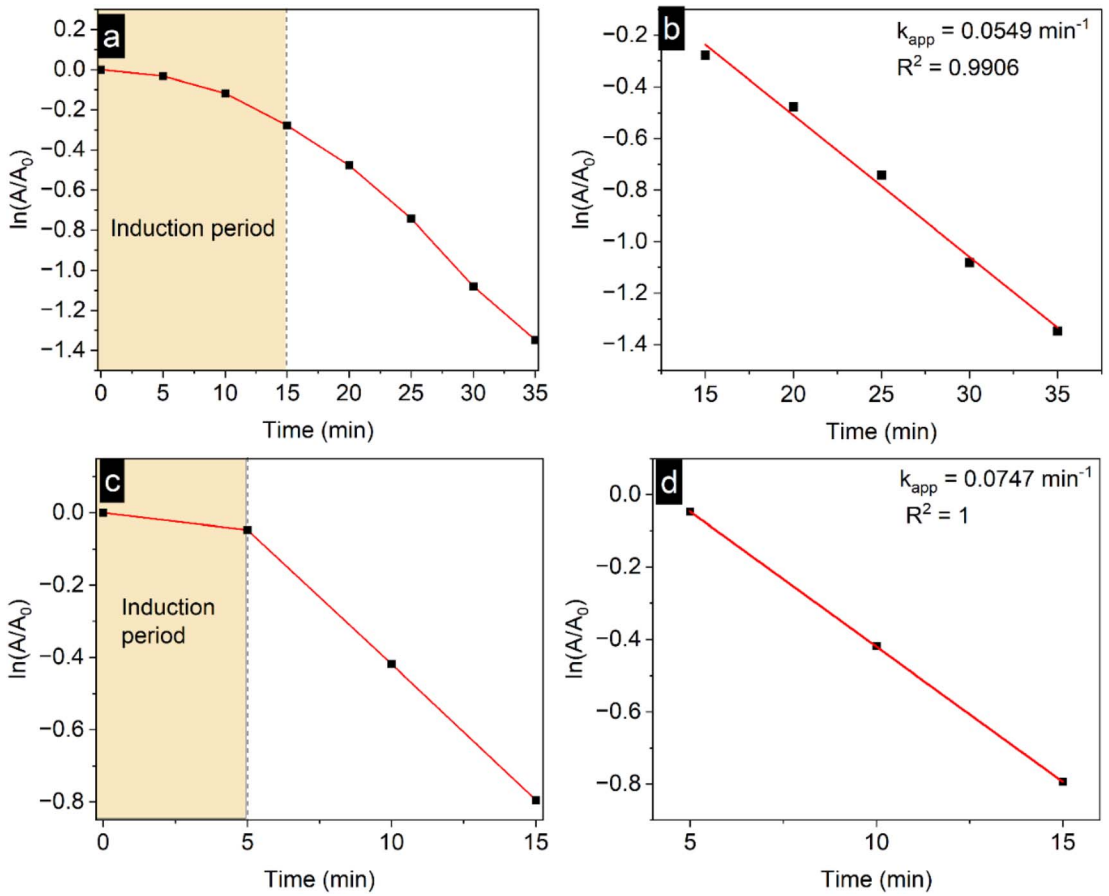

Fig. 9 Reduction kinetics of 4-nitrophenol: (a) and (b) in the presence of $NaBH_4$ stabilized by NaOH; (c) and (d) $NaBH_4$ without stabilization.

Table 4 Comparison of some bio-NCs for the reduction of 4-nitrophenol

Catalyst material	Molar ratio $NaBH_4$/4-nitrophenol	Amount of catalyst[a] (wt%)	k_{app} (min^{-1})	k' (min^{-1} mg^{-1})	Ref.
Eggshell/Cu	100	36.5	1.74	0.35	19
Eggshell membrane/Cu/Fe_2O_4	0.22	92.3	0.75	0.07	36
Eggshell/CuO/ZnO	660	98.6	0.20	0.01	37
Modified eggshell membrane/Cu/Ag	660	99.5	0.40	0.01	38
Soft calcite/Cu_2O/CuO	100	98.6	0.07	0.05	Current work

[a] Based on the weight of 4-nitrophenol.

and the emergence of a new peak close to 300 nm, corresponding to the 4-aminophenol product (Fig. 8). Two sets of reductions were carried out, one in the presence of $NaBH_4$ stabilized by NaOH and another without the stabilization of $NaBH_4$. Active reduction in the presence of $NaBH_4$ stabilized by NaOH took almost twice as long as the reduction with $NaBH_4$ alone, without stabilization. However, without the stabilization of $NaBH_4$, we observed more spectral interferences, possibly due to the more rapid evolution of hydrogen gas in the system. The rate of reduction was determined from the first order kinetic plot of $\ln(A_t/A_0)$ *vs.* t, where A_0 is the initial absorbance, A_t is the absorbance at a specific time interval and t is the time recorded in minutes. In the catalytic reduction of 4-nitrophenol in the presence of $NaBH_4$ stabilized by NaOH, active reduction was observed up to 35 min, with an induction period for the first 10 min. The induction period is often linked to the time required for the active surface of the catalytic NPs to form (surface restructuring) and reactant species to adsorb onto the catalyst surface, or for dissolved oxygen to be consumed.[34,35] The apparent rate constant (k_{app}) was determined to be 0.0549 min^{-1}. In the system without $NaBH_4$ stabilization, active reduction took place up to 15 min, with a 5 min induction period and a k_{app} of 0.0747 min^{-1} (Fig. 9).

The catalyst used in the reduction of 4-nitrophenol in the presence of $NaBH_4$ stabilized by NaOH did not show any indication of catalytic activity after the first cycle (Fig. S14 and Table S2†). After 35 min, there was only a very slight decline in the concentration of 4-nitrophenol. The catalyst used in the other system without $NaBH_4$ stabilization could be reused up to 3 cycles; however, for the second and third cycles, active reductions were observed up to 20 min. For the second cycle, no induction period was observed, and k_{app} was determined to be 0.0685 min^{-1}. For the third cycle, an induction period of 5 min was observed, and k_{app} was determined to be 0.1521 min^{-1} (Fig. S15†). The percentage of consumed 4-nitrophenol seemed to increase from cycle 1–3 (Table S2†). This observation may be due to the simultaneous reduction of the catalyst in earlier cycles. In the first reduction cycle, the catalyst turned black from its greyish-green colour, suggestive of the reduction of copper oxides in the catalyst to Cu(0) species. This resulted in the spent solution having a black tint (Fig. S16†). The black tint decreased with subsequent cycles, which also suggests that after multiple cycles, there was no further reduction of the catalyst. For the three cycles, the structural stability of the catalyst was retained throughout, as shown by SEM and TEM data (Fig. S17 and S18†).

A comparison of rate constant (k_{app}) and rate activity parameter (k') for our catalyst material to other similar metal biocomposites used for 4-nitrophenol reduction is shown in Table 4.

Conclusions

Biogenic calcium carbonate, including soft calcite, a calcium carbonate material from Newfoundland blue mussel shells, presents a huge opportunity for various kinds of surface modifications, which may be useful in achieving functionalities for different applications. Here we presented the syntheses of copper oxide nanocomposites using extracts from Newfoundland partridge berry. Two copper salts, $CuCl_2 \cdot 2H_2O$ and $CuSO_4$, were used in preparing these composites, and syntheses were conducted at either 80 °C or room temperature (25 °C) over 24 or 48 h, in the presence or absence of a basic environment. XPS data showed that the resulting nanoparticles incorporated on the surface of the soft calcite material were a combination of Cu_2O and CuO. Some of the composites had insufficient metal incorporation, making the nanoparticles undetectable by microscopy (SEM and TEM). For those with sufficient nanoparticle incorporation, the mean particle sizes of the nanoparticles were between 7 ± 0.2 and 28.2 ± 1.2 nm. Nanoparticle formation was more favoured with the use of $CuCl_2 \cdot 2H_2O$, and copper content was higher at 80 °C. Nanocomposites prepared at room temperature generally had low incorporation of copper species, except for composites prepared at room temperature over 48 h in a basic environment (high pH). This nanocomposite was chosen to demonstrate the catalytic ability of soft calcite nanocomposites to reduce 4-nitrophenol in the presence of sodium borohydride. 4-Nitrophenol could be reduced sufficiently within 20 min with an apparent rate constant of 0.0747 min^{-1}. This material could also be reused 3 times.

This research highlights the ongoing efforts of researchers to enhance the attractiveness of biomass for utilization in various processes aimed at ensuring the circularity of resources. These efforts are part of a broader initiative to effectively and sustainably manage by-products, which are an inevitable part of

many processes, including those in the food and agriculture industries. For future work, a broader scope of copper precursors, including the use of copper acetate, may be useful in changing the properties of these nanocomposites. Additionally, further catalytic investigations of these composites could be conducted on various other environmental contaminants, including aqueous formaldehyde.

Data availability

The data supporting this article have been included as part of the ESI.†

Author contributions

Conceptualization: F. M. K. and S. C. R.; methodology: S. C. R. and F. M. K.; characterization: S. C. R. and F. K.; writing – original draft: S. C. R.; writing – review and editing: S. C. R., F. M. K., F. K., and E. B. E.; supervision: F. M. K. and E. B. E.; funding acquisition: F. M. K. and E. B. E. All authors listed have agreed to the final version of this article and have made significant contributions.

Conflicts of interest

There are no conflicts to declare.

Acknowledgements

Funding was provided by NSERC of Canada, Canada Foundation for Innovation and Memorial University of Newfoundland (including Dr Liqin Chen for scholarship funds). FK acknowledges scholarship support from the NSERC CGS M program and Ontario Graduate Scholarship (OGS) program. We thank Memorial University's CREAIT Network for access to institutionally managed equipment, MDI Jade Software and the ICDD PDF-2 database. We also that Dr I. Ebralidze at Ontario Tech's Materials Characterization Facility for assistance with XPS measurements.

References

1 M. H. Azarian and W. Sutapun, *Front. Mater.*, 2022, **9**, 1024977.
2 S. Piras, S. Salathia, A. Guzzini, A. Zovi, S. Jackson, A. Smirnov, C. Fragassa and C. Santulli, *Materials*, 2024, **17**, 843.
3 V. Vandeginste, *Sustainable Mater. Technol.*, 2021, **29**, e00317.
4 J. N. Murphy, C. M. Schneider, K. Hawboldt and F. M. Kerton, *Matter*, 2020, **3**, 2029–2041.
5 S. Christian-Robinson and F. M. Kerton, *Pure Appl. Chem.*, 2024, **96**(9), 1247–1255.
6 K. Z. Elwakeel, A. M. Elgarahy and S. H. Mohammad, *J. Environ. Chem. Eng.*, 2017, **5**, 578–587.
7 D. Mantovani, H. B. Quesada, R. de Souza Antônio, L. F. Cusioli, L. Nishi, A. Diório, P. F. Soares, R. Bergamasco and M. F. Vieira, *Desalin. Water Treat.*, 2020, **188**, 232–238.
8 H. Su, X. Guo, X. Zhang, Q. Zhang, D. Huang, L. Lin and X. Qiang, *Bioresour. Technol. Rep.*, 2022, **19**, 101124.
9 C. Triunfo, S. Gärtner, C. Marchini, S. Fermani, G. Maoloni, S. Goffredo, J. Gomez Morales, H. Cölfen and G. Falini, *ACS Omega*, 2022, **7**, 43992–43999.
10 Y.-Q. Niu, J.-H. Liu, C. Aymonier, S. Fermani, D. Kralj, G. Falini and C.-H. Zhou, *Chem. Soc. Rev.*, 2022, **51**, 7883–7943.
11 J. Qiu, J. Lyu, J. Yang, K. Cui, H. Liu, G. Wang and X. Liu, *Part. Part. Syst. Charact.*, 2024, 2400097.
12 Y. Li, S. Xin, Y. Bian, K. Xu, C. Han and L. Dong, *Int. J. Biol. Macromol.*, 2016, **85**, 63–73.
13 B. Pant, M. Park, H.-Y. Kim and S.-J. Park, *J. Alloys Compd.*, 2017, **699**, 73–78.
14 N. Fahmi Khairol, N. Sapawe and M. Danish, *Mater. Today*, 2019, **19**, 1255–1260.
15 Y. Guo, D.-P. Yang, M. Liu, X. Zhang, Y. Chen, J. Huang, Q. Li and R. Luque, *J. Mater. Chem. A*, 2019, **7**, 8832–8844.
16 Q. Ding, Z. Kang, L. Cao, M. Lin, H. Lin and D.-P. Yang, *Appl. Surf. Sci.*, 2020, **510**, 145526.
17 C. Qian, J. Yin, J. Zhao, X. Li, S. Wang, Z. Bai and T. Jiao, *Colloids Surf., A*, 2021, **610**, 125752.
18 N. S. Naik, S. Divakar, J. M. S., S. Budagumpi, R. G. Balakrishna and M. Padaki, *RSC Sustainability*, 2024, **2**, 1246–1268.
19 M. Nasrollahzadeh, S. M. Sajadi and A. Hatamifard, *Appl. Catal., B*, 2016, **191**, 209–227.
20 S. M. Sajadi, K. Kolo, S. M. Abdullah, S. M. Hamad, H. S. Khalid and A. T. Yassein, *Surf. Interfaces*, 2018, **13**, 205–215.
21 Y. Guo, Y. Sun, D.-P. Yang, J. Dai, Z. Liu, Y. Chen, J. Huang and Q. Li, *ACS Appl. Mater. Interfaces*, 2020, **12**, 2469–2480.
22 M. Baláž, M. Casas-Luna, A. Augustinyak, Ľ. Tkáčiková, K. Szmuc, M. Kováčová, L. Čelko and Y. Shpotyuk, *Appl. Nanosci.*, 2022, **12**, 1899–1916.
23 A. Naeimi, F. E. Ghadi, S. M. Saadatkhah and M. Honarmand, *J. Mol. Struct.*, 2022, **1259**, 132690.
24 K. S. Bhullar and H. P. V. Rupasinghe, *Food Chem.*, 2015, **168**, 595–605.
25 NIST X-ray Photoelectron Spectroscopy Database, **https://srdata.nist.gov/xps/**, accessed 5 March 2025.
26 H. R. El-Seedi, R. M. El-Shabasy, S. A. M. Khalifa, A. Saeed, A. Shah, R. Shah, F. J. Iftikhar, M. M. Abdel-Daim, A. Omri, N. H. Hajrahand, J. S. M. Sabir, X. Zou, M. F. Halabi, W. Sarhan and W. Guo, *RSC Adv.*, 2019, **9**, 24539–24559.
27 A. M. E. Shafey, *Green Process. Synth.*, 2020, **9**, 304–339.
28 A. Labanni, M. Nasir and S. Arief, *Materials Today Sustainability*, 2023, **24**, 100526.
29 K. M. Rajesh, B. Ajitha, Y. Ashok Kumar Reddy, Y. Suneetha and P. Sreedhara Reddy, *Mater. Today: Proc.*, 2016, **3**, 1985–1991.
30 R. Amjad, B. Mubeen, S. S. Ali, S. S. Imam, S. Alshehri, M. M. Ghoneim, S. I. Alzarea, R. Rasool, I. Ullah, M. S. Nadeem and I. Kazmi, *Polymers*, 2021, **13**, 4364.

31 R. Alipour Moghadam Esfahani, F. Kong, K. Black-Araujo, L. J. Easton, I. I. Ebralidze and E. B. Easton, *Electrochim. Acta*, 2023, **438**, 141564.
32 S. W. Goh, A. N. Buckley, R. N. Lamb, R. A. Rosenberg and D. Moran, *Geochim. Cosmochim. Acta*, 2006, **70**, 2210–2228.
33 C. F. Holder and R. E. Schaak, *ACS Nano*, 2019, **13**, 7359–7365.
34 P. Hervés, M. Pérez-Lorenzo, L. M. Liz-Marzán, J. Dzubiella, Y. Lu and M. Ballauff, *Chem. Soc. Rev.*, 2012, **41**, 5577.
35 Y. R. Mejía and N. K. Reddy Bogireddy, *RSC Adv.*, 2022, **12**, 18661–18675.
36 Y. Zhang, Y. Chen, Z.-W. Kang, X. Gao, X. Zeng, M. Liu and D.-P. Yang, *Colloids Surf., A*, 2021, **612**, 125874.
37 X. Zhang, X. He, Z. Kang, M. Cui, D.-P. Yang and R. Luque, *ACS Sustain. Chem. Eng.*, 2019, **7**, 15762–15771.
38 Y. Xin, C. Li, J. Liu, J. Liu, Y. Liu, W. He and Y. Gao, *R. Soc. Open Sci.*, 2018, **5**, 180532.